



Quasiparticle Interference, Quasiparticle Interactions, and the Origin of the Charge Density Wave in $2H\text{-NbSe}_2$

C. J. Arguello,¹ E. P. Rosenthal,¹ E. F. Andrade,¹ W. Jin,² P. C. Yeh,² N. Zaki,³ S. Jia,⁴ R. J. Cava,⁴ R. M. Fernandes,⁵ A. J. Millis,¹ T. Valla,⁶ R. M. Osgood, Jr.,^{3,4} and A. N. Pasupathy¹

¹*Department of Physics, Columbia University, New York, New York 10027, USA*

²*Department of Applied Physics and Applied Math, Columbia University, New York, New York 10027, USA*

³*Department of Electrical Engineering, Columbia University, New York, New York 10027, USA*

⁴*Department of Chemistry, Princeton University, Princeton, New Jersey 08540, USA*

⁵*School of Physics and Astronomy, University of Minnesota, Minneapolis, Minnesota 55455, USA*

⁶*Brookhaven National Laboratory, Upton, New York 11973, USA*

(Received 19 August 2014; published 21 January 2015)

We show that a small number of intentionally introduced defects can be used as a spectroscopic tool to amplify quasiparticle interference in $2H\text{-NbSe}_2$ that we measure by scanning tunneling spectroscopic imaging. We show, from the momentum and energy dependence of the quasiparticle interference, that Fermi surface nesting is inconsequential to charge density wave formation in $2H\text{-NbSe}_2$. We demonstrate that, by combining quasiparticle interference data with additional knowledge of the quasiparticle band structure from angle resolved photoemission measurements, one can extract the wave vector and energy dependence of the important electronic scattering processes thereby obtaining direct information both about the fermiology and the interactions. In $2H\text{-NbSe}_2$, we use this combination to confirm that the important near-Fermi-surface electronic physics is dominated by the coupling of the quasiparticles to soft mode phonons at a wave vector different from the charge density wave ordering wave vector.

DOI: 10.1103/PhysRevLett.114.037001

PACS numbers: 74.55.+v, 71.45.Lr, 72.10.Di, 79.60.-i

In many complex materials, including the two dimensional cuprates [1–5], the pnictides [6], and the dichalcogenides, the electronic ground state may spontaneously break the translational symmetry of the lattice. Such density wave ordering can arise from Fermi surface nesting, from strong electron-electron interactions, or from interactions between the electrons and other degrees of freedom in the material, such as phonons. The driving force behind the formation of the spatially ordered states and the relationship of these states to other electronic phases, such as superconductivity, remains hotly debated.

Scanning tunneling spectroscopy (STS) has emerged as a powerful technique for probing the electronic properties of such ordered states at the nanoscale [3–5] due to its high energy and spatial resolution. The position dependence of the current I -voltage V characteristics measured in STS experiments maps the energy dependent local density of states $\rho(\mathbf{r}, E)$ [7,8]. Correlations between the $\rho(\mathbf{r}, E)$ at different points at a given energy reveal the pattern of standing waves produced when electrons scatter off of impurities [9]. These quasiparticle interference (QPI) features may be analyzed to reveal information about the momentum space structure of the electronic states [10]. The intensity of the QPI signals as a function of energy and momentum also contains information about the electronic interactions in the material [11,12].

In this Letter, we take the ideas further, showing how impurities can be used intentionally to enhance QPI signals

in STS experiments and how the combination of the enhanced QPI signals with electronic spectroscopic information available in angle-resolved photoemission (ARPES) measurements can be used to gain insight into the physics underlying electronic symmetry breaking and quasiparticle interactions. By observing the electronic response to the addition of dilute, weak impurities to the charge density wave material $2H\text{-NbSe}_2$ we directly measure the dominant electronic scattering channels. We show, conclusively, that Fermi surface nesting does not drive charge density wave (CDW) formation and that the dominant quasiparticle scattering arises from soft-mode phonons.

Following previous work [13], our theoretical analysis begins from a standard relation between the current-voltage characteristic dI/dV at position \mathbf{r} and voltage difference $V = E$ and the electron Green's function G , valid if the density of states in the tip used in the STS experiment is only weakly energy dependent

$$\frac{dI(\mathbf{r}, E)}{dV} = \text{Tr} \left[\mathbf{M}^{\text{tun}} \frac{[\mathbf{G}(\mathbf{r}, \mathbf{r}, E - i\delta) - \mathbf{G}(\mathbf{r}, \mathbf{r}, E + i\delta)]}{2\pi i} \right]. \quad (1)$$

Here, \mathbf{M} is a combination of the tunneling matrix element and wave functions (see Supplemental Material [14]); \mathbf{M} and \mathbf{G} are matrices in the space of band indices.

To calculate the changes in dI/dV induced by impurities, we observe that, in the presence of a single impurity placed at position \mathbf{R}_a , the electron Green's function is changed from the pure system form G to $\tilde{\mathbf{G}}$ given by

$$\tilde{\mathbf{G}}(\mathbf{r}, \mathbf{r}', E) = \mathbf{G}(\mathbf{r} - \mathbf{r}', E) + \int d\mathbf{r}_1 d\mathbf{r}_2 \mathbf{G}(\mathbf{r} - \mathbf{r}_1, E) \mathbf{T}(\mathbf{r}_1 - \mathbf{R}_a, \mathbf{r}_2 - \mathbf{R}_a, E) \mathbf{G}(\mathbf{r}_2 - \mathbf{r}', E). \quad (2)$$

Here, $\mathbf{T}(\mathbf{r}, \mathbf{r}', E)$ is the T matrix describing electron-impurity scattering as renormalized by electron-electron interactions. It is a matrix in the space of band indices, and we suppress spin indices, which play no role in our considerations.

Assuming (see Supplemental Material [14]) that \mathbf{M} is structureless (couples all band indices equally), Fourier transforming, and assuming that interference between different impurities is not important gives for the impurity-induced change in the tunneling current

$$\delta \frac{dI(\mathbf{k}, E)}{dV} = \left(\frac{1}{v} \sum_a e^{i\mathbf{k} \cdot \mathbf{R}_a} \right) \frac{\Phi_{\mathbf{k}}(E - i\delta) - \Phi_{\mathbf{k}}(E + i\delta)}{2\pi i}, \quad (3)$$

with v the volume of the systems and the scattering function of complex argument z given in the band basis in which \mathbf{G} is diagonal as

$$\Phi_{\mathbf{k}}(z) = \sum_{nm} \int G_{\mathbf{p}}^n(z) T_{\mathbf{p}, \mathbf{p}+\mathbf{k}}^{nm}(z) G_{\mathbf{p}+\mathbf{k}}^m(z) d\mathbf{p}. \quad (4)$$

At this stage no assumption has been made about interactions.

From Eq. (3), we see that structure in $\delta dI(\mathbf{k}, E)/dV$ can arise from structure in the combination $G_{\mathbf{p}} G_{\mathbf{p}+\mathbf{k}}$ of electron propagators (Fermi surface nesting) or from structure in the T matrix, the latter arising either from properties of the impurity or from interactions involving the scattered electrons. Combining an STS measurement with an independent determination of G (for example by ARPES) allows the two physical processes to be distinguished. However, a direct analysis of Eq. (3) requires precise measurement of the positions of all of the impurities so that the $\sum_a e^{i\mathbf{k} \cdot \mathbf{R}_a}$ factor can be divided out. This is impractical at present, so we focus on $|\delta dI(\mathbf{k}, E)/dV|$ where, for dilute randomly placed impurities, the prefactor can be replaced by the square root of the impurity density. Equation (3) can be further simplified if one assumes that the T matrix depends primarily on the momentum transfer k and has negligible imaginary parts (i.e., scattering phase shift near 0 or π). Such an assumption is particularly appropriate when the scattering arises from weakly scattering uncharged point impurities. We find

$$\left| \delta \frac{dI(\mathbf{k}, E)}{dV} \right| = \sqrt{n_{\text{imp}}} \left| \sum_{nm} B^{nm}(\mathbf{k}, E) T_{\mathbf{k}}^{nm}(E) \right|, \quad (5)$$

with

$$B^{nm}(\mathbf{k}, E) = \sum_p \frac{G_{\mathbf{p}}^n(E - i\delta) G_{\mathbf{p}+\mathbf{k}}^m(E - i\delta) - (\delta \leftrightarrow -\delta)}{2\pi i}. \quad (6)$$

An integral of B over the occupied states yields the components of the noninteracting (Lindhard) susceptibility [11] (see Supplemental Material [14]),

$$\chi_0^{nm}(\mathbf{k}) \propto \int_{-\infty}^{\infty} \frac{dE}{\pi} f(E) [B^{nm}(\mathbf{k}, E) + B^{mn}(\mathbf{k}, E)], \quad (7)$$

where f is the Fermi function. This observation permits an interesting analysis.

If the impurity scattering potential V_{imp} is structureless and weak, a measurement of the QPI then directly yields the susceptibility. Conversely, if the impurities are known to be weak, differences between the measured QPI intensity and the Lindhard susceptibility (obtained from a non-interacting calculation) reveal the effects of interactions, which appear formally as a ‘‘vertex correction’’ of the basic impurity-quasiparticle scattering amplitude V_{imp} (see Supplemental Material [14]).

We apply these concepts to $2H\text{-NbSe}_2$, a quasi-2D transition metal dichalcogenide, that displays a CDW phase transition below $T_{\text{CDW}} \approx 33$ K [15–17]. The physics of this ordered state is still under debate. While some experiments point to an important role of Fermi surface (FS) nesting [18,19], perhaps accompanied by a van Hove singularity [20,21], an alternative scenario argues that the nesting of the FS is not strong enough to produce the CDW instability [22,23], and proposes that a strong electron-phonon coupling [24,25] is responsible. ARPES experiments do not detect a strong effect of the CDW order on the near-FS states.

No signatures of QPI have been detected in previous STS studies of NbSe_2 , presumably due to the lack of sufficient scattering centers in the pristine material. To enhance the QPI signal, we introduced dilute sulfur doping to pristine NbSe_2 ($\text{NbSe}_{(2-x)}\text{S}_x$). The $\text{NbSe}_{2-x}\text{S}_x$ crystals used in this work were grown by the self-transport method starting from stoichiometric proportions of elemental Nb, Se, and S powders over the period of one week in a temperature gradient of 950 to 900 °C. S and Se are isovalent atoms, so no charge doping arises from the substitution. Furthermore, the similarity of the calculated band structures of NbSe_2 and NbS_2 shows that the bare scattering potential induced

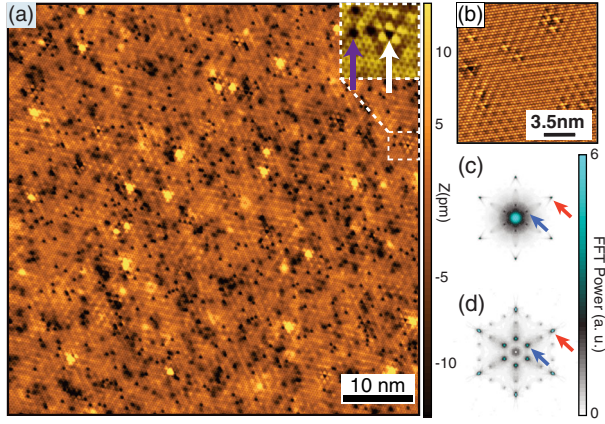


FIG. 1 (color online). (a) Large area topographic image of $\text{NbSe}_{(2-x)}\text{S}_x$ below T_{CDW} , showing inhomogeneous patches of CDW. Zoomed-in region (inset) shows a sulfur dopant (purple arrow) and a vacancy (white arrow); the CDW amplitude is strongly enhanced near the vacancy. (b) Topographic image of pristine NbSe_2 where the CDW is seen in all the field of view. (c) FFT of the topographic image shown in (a). The inner peaks (arrow closer to origin, blue online) correspond to the CDW, the outer peaks (arrow closer to zone boundary, red online) are the atomic Bragg peaks. (d) FFT of the topography of the image shown in (b).

by the substitution $\text{Se} \rightarrow \text{S}$ is weak. We have estimated the S-defect concentration to be approximately 1% from STM topographic images. In Fig. 1(a), we show a typical topographic image taken at 27 K ($T < T_{\text{CDW}}$) that displays the S defects as well as a few Se vacancies. In Fig. 1(b), we show a topographic image of pristine NbSe_2 in the CDW state for comparison. The CDW persists in the S-doped material as evidenced by its coverage across the entire sample, although the doped material is clearly less homogeneous than the pristine sample. This is also evident in the 2D fast Fourier transform (FFT) of the topographic images for the doped [Fig. 1(c)] and pristine [Fig. 1(d)] samples. Well defined CDW peaks at $\mathbf{k}_{\text{CDW}} = \mathbf{k}_{\text{Bragg}}/3$ are seen in the FFT for the pristine sample. These peaks broaden in the doped material, though the periodicity of the CDW does not change. Interestingly, in both materials, the CDW is enhanced in the neighborhood of the Se vacancies, and the S defects do not affect either the phase or amplitude of the CDW [see inset in Fig 1(a)].

Figure 2(a) shows a typical STS map $(dI/dV)(\mathbf{r}, E)$ in real space. Figure 2(b) shows the square root of the Fourier power of the dI/dV maps, $|(dI/dV)(\mathbf{k}, E)|$ at four different energies. These Fourier transforms (FTs) have been symmetrized to reflect the sixfold symmetry of the system. Two important features are present in the Fourier transforms for all probed energies. First, there are peaks at $\mathbf{k} \approx \mathbf{k}_{\text{Bragg}}/3$ [black arrows in Fig. 2(b) at all energies measured by STS, see Supplemental Material [14]]. This feature has been seen before in the pristine sample [26] and is a consequence of the CDW order. A second feature occurs along the same

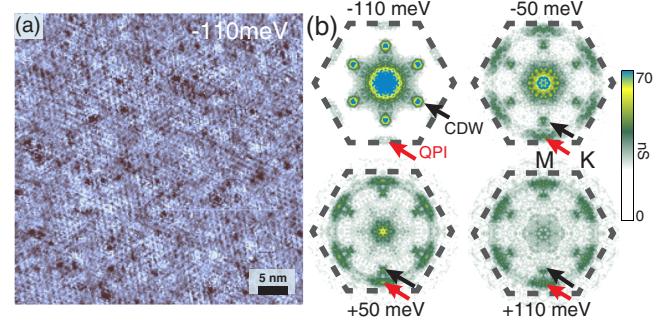


FIG. 2 (color online). (a) Real space dI/dV map at $E = -110$ meV. The readily visible triangular lattice arises from the charge density wave (additional real space STS images shown in the Supplemental Material [14]). (b) Absolute value of the FFT of dI/dV maps at different energies showing nondispersing CDW peak (heavy arrow, black online) and QPI peaks dispersing with energy (light arrow, red online). Maps have been rotationally symmetrized as described in the main text.

direction as the CDW wave vector but at an energy-dependent position. Since this feature disperses in k as E is changed, we identify it as a QPI signal. Thus, the light doping introduced in the system successfully enhances the QPI signal while not altering the electronic structure of NbSe_2 . The QPI dispersion is not completely linear, and the subtle kinks in the dispersion could indicate coupling to electronic scattering channels near the Fermi level. The presence of these kinks does not affect our main conclusions and future measurements will focus on quantifying these nonlinearities and distinguishing them from the bare dispersion of the bands.

From Fig. 2(b), we see that the QPI peaks are located at wave vectors close to the Brillouin zone edge for $E = -110$ meV and move towards the zone center with increasing energy. We see, however, that, for all energies presented in this Letter, the QPI peaks remain far from the

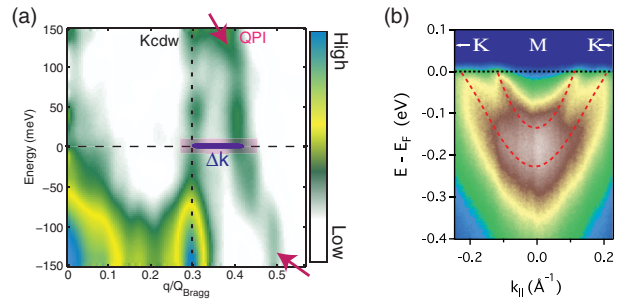


FIG. 3 (color online). (a) Line cut of the dI/dV maps in Fourier space along the $\Gamma - M$ direction. The dashed line is a guide for the eye highlighting the position of the CDW ordering vector while the heavy line and shading (pink online) highlights the separation between the QPI intensity and the CDW wave vector at the Fermi energy. (b) ARPES (photon energy ≈ 23 eV) line cut along the $K - M - K$ direction. The dotted line is the tight-binding fit to the data.

CDW wave vector. This is illustrated more clearly in Fig. 3(a) which presents a line cut of the STS data along the $\Gamma - M$ direction for each one of the energy slices of the STS maps. At the Fermi energy, the QPI signal is separated from the CDW signal by $\Delta\mathbf{k} \approx \frac{1}{3}\mathbf{k}_{\text{CDW}}$. From the QPI dispersion, it is evident that k_{QPI} would reach k_{CDW} at an energy well above the Fermi level.

Combining ARPES and STS measurements allows us to extract important additional information about the nature of scattering near the Fermi level in the CDW state of NbSe₂. Representative ARPES measurements are presented in Fig. 3(b). Comparison to similar data obtained on the pristine material [19,27] revealed no significant changes in the band dispersion, further confirming that study of the lightly S-doped system reveals information relevant to pristine NbSe₂. We fit our ARPES measurements in Fig. 3(b) to a two-band, five nearest-neighbor, tight-binding model similar to the one presented in Ref. [28] (see Supplemental Material [14] for details). This fit captures the primarily two-dimensional Nb-derived bands that are believed to dominate the physics. In calculated band structures, an additional Se-derived band is nearly degenerate with the Nb-derived bands near the Γ point, but disperses away as either k_z or the in-plane k is increased; this band is typically not observed in ARPES experiments, most probably because of broadening associated with strong k_z dispersion and, for the same reason, will make a much less important contribution to the QPI (see Supplemental Material [14] for the details of the bands, parameters of the fit, and discussion of the Se-derived states). The fit indicates a moderate-strong (factor of 2–3) renormalization of the observed bands relative to the calculated [22,23] bands, as previously noted [28]. Using this band structure, we then calculate G and, hence, $B^{mn}(\mathbf{k}, E)$ from Eq. (6). Figure 4(a) shows the result of the calculation as well as the FT-STs measurements at the same energies (see Supplemental Material [14] for comparisons between FT-STs and B at additional energies). A highly structured B is found, but the structures have only an indirect relation to the experimental QPI spectra. In particular, B exhibits highest intensity near the K point of the Brillouin zone, where the QPI features are weak, and does not exhibit significant intensity where the QPI features are strongest.

To further characterize the differences between the quasiparticle band structure and the QPI, we assume that the T matrix couples all states equally [$T_{\mathbf{k}}^{mn}(E) = T_{\mathbf{k}}(E)$ independent of band indices mn] and construct an experimental estimate of $T_{\mathbf{k}}(E)$ from Eq. (5) by dividing the measured $|\delta dI(\mathbf{k}, E)/dV|$ by the calculated $\sum_{mn} B^{nm}(\mathbf{k}, E)$. The resulting $|T_{\mathbf{k}}(E)|$ is shown in Fig. 4(b). The strong and nondispersing peak seen in $T_{\mathbf{k}}(E)$ at the CDW wave vector [indicated by the green arrows in Fig. 4(b)] is similar to the structure factors seen in electron diffraction experiments [29,30]. It is caused by the

deformation of the band structure due to the periodic potential arising from the CDW ordering. Its lack of dispersion shows directly that this feature in our STS signal does not arise from quasiparticles.

We now consider the structure highlighted as a strong peak in T near the zone edge in the $\Gamma - M$ direction indicated by the purple arrows in Fig. 4(b). All available evidence suggests that the potential induced by the S dopants is weak and structureless, so that the enhancement is an interaction effect. The strong momentum dependence of $|T|$ indicates that the intensity variation of the STS signal is not explained by the quasiparticle band structure. However, it is significant that, at all measured energies, the strong peak in T lies within the $|\mathbf{k}|$ region delineated by the group of approximately concentric circles seen in the calculated B [denoted by the black boxes in Fig. 4(a)]. The main contribution to these circles arises from $2k_F$ backscattering across each of the Fermi surfaces. This suggests that the observed QPI arises from an enhancement of backscattering [31] by a strongly direction-dependent interaction [32]. Available calculations [24,33] suggest that soft acoustic phonons with wave vectors along the $\Gamma - M$ direction are strongly coupled to electrons for a wide range of $|\mathbf{k}|$. By contrast, the high intensity regions in B near the K point arise from approximate nesting of the Fermi surfaces centered at Γ and K ; that these are not seen in the measured

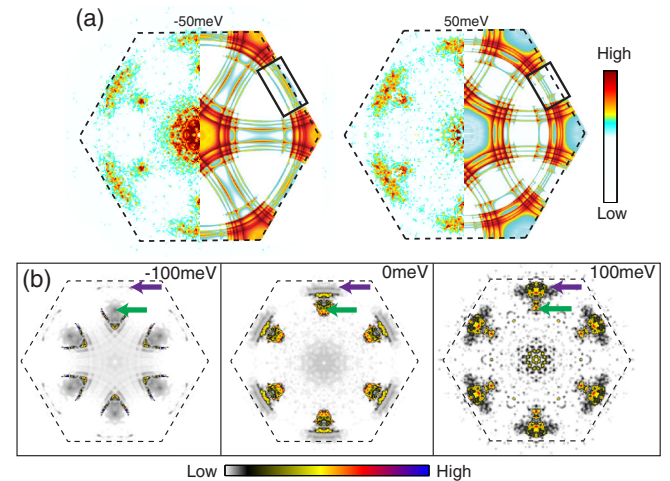


FIG. 4 (color online). (a) Absolute value of FFT of experimental (left half of image) and theoretical (right half of image) dI/dV map at $E = -50$ meV (left image) and $E = 50$ meV (right image). Theoretical images calculated as $\sum_{mn} B^{nm}(\mathbf{k}, E)$ using Eq. (6) with tight-binding model bands obtained from fits to ARPES measurements as described in the Supplemental Material [14]. The dotted line is the edge of the first Brillouin zone. The black boxes indicate the areas in \mathbf{k} space where the T matrix is strongly peaked. (b) $|T_{\mathbf{k}}(E)|$ calculated from the STS data using Eq. (5) for -100 meV (left), Fermi energy (center), and 100 meV (right). The green arrow points to the position of the CDW wave vector, the purple arrow points to the dispersing feature in the T matrix.

QPI again confirms that nesting is not enhanced by interactions and is not important in this material. We, therefore, propose that the observed QPI signal arises from a renormalization of a structureless impurity potential by the electron-phonon interaction.

In summary, we used dilute doping of NbSe₂ with isovalent S atoms to enhance the QPI signal and, by combining STS and ARPES measurements, were able to show that the QPI signal measures more than just the fermiology of the material. We were able to confirm that the CDW does not arise from Fermi-surface nesting, and we identified an important quasiparticle interaction, most likely of electron-phonon origin. Our approach reveals that the response to deliberately induced dopants is an important spectroscopy of electronic behavior. We expect it can be extended to many other systems.

This work was supported by the National Science Foundation (NSF) under Grant No. DMR-1056527 (E. P. R., A. N. P.) and by the Materials Interdisciplinary Research Team Grant No. DMR-1122594 (A. N. P., A. J. M.). Salary support was also provided by the U.S. Department of Energy under Contracts No. DE-FG 02-04-ER-46157 (W. J., P. C. Y., N. Z., and R. M. O.). R. M. F. is supported by the U.S. Department of Energy under Award No. DE-SC0012336. ARPES research carried out at National Synchrotron Light Source, Brookhaven National Laboratory is supported by the U.S. Department of Energy, Office of Basic Energy Sciences (DOE-BES), under Contract No. DE-AC02-98CH10886. The crystal growth work at Princeton University was funded by DOE-BES Grant No. DE-FG02-98ER45706. A. J. M. acknowledges the hospitality of the Aspen Center for Physics (supported by NSF Grant No. 1066293) for hospitality during the conception and writing of this Letter.

-
- [1] R. Comin *et al.*, *Science* **343**, 390 (2014).
 - [2] E. H. da Silva Neto *et al.*, *Science* **343**, 393 (2014).
 - [3] Y. Kohsaka *et al.*, *Science* **315**, 1380 (2007).
 - [4] M. Vershinin, S. Misra, S. Ono, Y. Abe, Y. Ando, and A. Yazdani, *Science* **303**, 1995 (2004).
 - [5] W. D. Wise, M. C. Boyer, K. Chatterjee, T. Kondo, T. Takeuchi, H. Ikuta, Y. Wang, and E. W. Hudson, *Nat. Phys.* **4**, 696 (2008).
 - [6] E. P. Rosenthal, E. F. Andrade, C. J. Arguello, R. M. Fernandes, L. Y. Xing, X. C. Wang, C. Q. Jin, A. J. Millis, and A. N. Pasupathy, *Nat. Phys.* **10**, 225 (2014).
 - [7] J. Tersoff and D. R. Hamann, *Phys. Rev. B* **31**, 805 (1985).
 - [8] J. Li, W.-D. Schneider, and R. Berndt, *Phys. Rev. B* **56**, 7656 (1997).
 - [9] M. F. Crommie, C. P. Lutz, and D. M. Eigler, *Nature (London)* **363**, 524 (1993).

- [10] K. McElroy, R. W. Simmonds, J. E. Hoffman, D. Lee, J. Orenstein, H. Eisaki, S. Uchida, and J. C. Davis, *Nature (London)* **422**, 592 (2003).
- [11] S. A. Kivelson, I. P. Bindloss, E. Fradkin, V. Oganesyan, J. M. Tranquada, A. Kapitulnik, and C. Howald, *Rev. Mod. Phys.* **75**, 1201 (2003).
- [12] Y. B. Kim and A. J. Millis, *Phys. Rev. B* **67**, 085102 (2003).
- [13] G. A. Fiete and E. J. Heller, *Rev. Mod. Phys.* **75**, 933 (2003).
- [14] See Supplemental Material at <http://link.aps.org/supplemental/10.1103/PhysRevLett.114.037001> for details of the theoretical formulas used in the Letter, details of the tight binding fits to photoemission data, calculation of the partial susceptibility from STM data, real space STS maps, comparisons between STS and photoemission at different energies, and fits to the CDW wavelength as a function of energy from STS maps.
- [15] D. E. Moncton, J. D. Axe, and F. J. DiSalvo, *Phys. Rev. Lett.* **34**, 734 (1975).
- [16] J. A. Wilson, F. J. di Salvo, and S. Mahajan, *Adv. Phys.* **24**, 117 (1975).
- [17] R. Coleman, B. Giambattista, P. Hansma, A. Johnson, W. McNairy, and C. Slough, *Adv. Phys.* **37**, 559 (1988).
- [18] T. Straub, T. Finteis, R. Claessen, P. Steiner, S. Hüfner, P. Blaha, C. S. Oglesby, and E. Bucher, *Phys. Rev. Lett.* **82**, 4504 (1999).
- [19] S. V. Borisenko *et al.*, *Phys. Rev. Lett.* **102**, 166402 (2009).
- [20] T. M. Rice and G. K. Scott, *Phys. Rev. Lett.* **35**, 120 (1975).
- [21] W. C. Tonjes, V. A. Greanya, R. Liu, C. G. Olson, and P. Molinié, *Phys. Rev. B* **63**, 235101 (2001).
- [22] K. Rossnagel, O. Seifarth, L. Kipp, M. Skibowski, D. Voß, P. Krüger, A. Mazur, and J. Pollmann, *Phys. Rev. B* **64**, 235119 (2001).
- [23] M. D. Johannes, I. I. Mazin, and C. A. Howells, *Phys. Rev. B* **73**, 205102 (2006).
- [24] F. Weber, S. Rosenkranz, J.-P. Castellan, R. Osborn, R. Hott, R. Heid, K.-P. Bohnen, T. Egami, A. H. Said, and D. Reznik, *Phys. Rev. Lett.* **107**, 107403 (2011).
- [25] C. M. Varma and A. L. Simons, *Phys. Rev. Lett.* **51**, 138 (1983).
- [26] C. J. Arguello *et al.*, *Phys. Rev. B* **89**, 235115 (2014).
- [27] D. S. Inosov, V. B. Zabolotnyy, D. V. Evtushinsky, A. A. Kordyuk, B. Bchner, R. Follath, H. Berger, and S. V. Borisenko, *New J. Phys.* **10**, 125027 (2008).
- [28] D. J. Rahn, S. Hellmann, M. Kalläne, C. Sohrt, T. K. Kim, L. Kipp, and K. Rossnagel, *Phys. Rev. B* **85**, 224532 (2012).
- [29] C. Chen, *Solid State Commun.* **49**, 645 (1984).
- [30] P. Williams, C. Scruby, and G. Tatlock, *Solid State Commun.* **17**, 1197 (1975).
- [31] E. H. da Silva Neto, C. V. Parker, P. Aynajian, A. Pushp, A. Yazdani, J. Wen, Z. Xu, and G. Gu, *Phys. Rev. B* **85**, 104521 (2012).
- [32] T. Valla, A. V. Fedorov, P. D. Johnson, P.-A. Glans, C. McGuinness, K. E. Smith, E. Y. Andrei, and H. Berger, *Phys. Rev. Lett.* **92**, 086401 (2004).
- [33] F. Weber, R. Hott, R. Heid, K.-P. Bohnen, S. Rosenkranz, J.-P. Castellan, R. Osborn, A. H. Said, B. M. Leu, and D. Reznik, *Phys. Rev. B* **87**, 245111 (2013).